ACS APPLIED MATERIALS & INTERFACES

Research Article

www.acsami.org

Photocatalytic H_2 Evolution from Water–Methanol System by Anisotropic $InFeO_3(ZnO)_m$ Oxides without Cocatalyst in Visible Light

Soumya B. Narendranath,[†] Ashok Kumar Yadav,[‡] Dibyendu Bhattacharyya,[‡] Shambu Nath Jha,[‡] and R. Nandini Devi*[,†]

[†]Catalysis Division, CSIR-National Chemical Laboratory, Dr. Homi Bhabha Road, Pune 411008, India

[‡]Atomic and Molecular Physics Division, Bhabha Atomic Research Centre, Trombay, Mumbai 400085, India

Supporting Information

ABSTRACT: $InFeO_3(ZnO)_m$ series of oxides are found to give unprecedented H_2 evolution from water–methanol mixtures without using any cocatalysts. This family of compounds has an anisotropically layered structure in which Zn/FeO_n polyhedra are sandwiched between InO_6 octahedral layers. Local structure characterization by X-ray absorption spectroscopy reveals that Zn coordination changes from pentacoordinated to tetrahedral geometry across the series, whereas Fe geometry remains trigonal bipyramidal in all the compounds. This peculiar structure is conducive for a spatial separation of photogenerated charges reducing recombination losses. Band gap energies calculated from absorption spectra indicate potential visible light activity, and this may be due to the orbital mixing of Fe 3d and O 2p as revealed by pre-edge features of X-ray absorption spectra. Band positions are also advantageously placed for a visible light H_2 generation and is indeed found to be the case in methanol-assisted water splitting with standardized hydrogen evolution of ~19.5 mmol g^{-1} h^{-1} for all the catalysts.

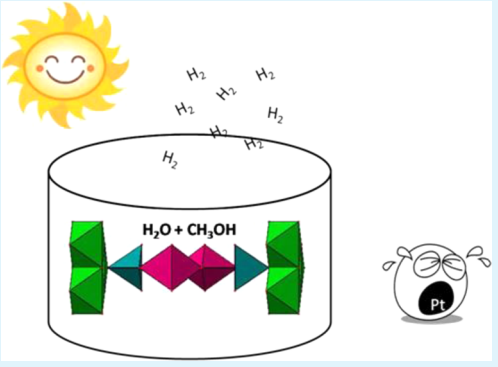

KEYWORDS: *$InFeO_3(ZnO)_m$, anisotropic structure, H_2 evolution, photocatalytic water splitting, layered oxide*

INTRODUCTION

Photocatalytic hydrogen production from water is one of the most promising ways to generate clean energy.[1−4] Water splitting using semiconductor powder catalysts is the preferred process currently because of the simplicity and ease of handling. A suitable photocatalytic material should possess sufficiently small band gap for utilizing more abundant visible light region in the solar spectrum. Also the valence band and conduction band positions with respect to the reduction and oxidation potentials of water should be appropriate to drive overall water splitting.[5] On irradiation with light of appropriate energy, electrons and holes are generated in the bulk of the semiconductor particles, and they travel to the surface, eventually getting utilized in the reduction and oxidation reactions of water, respectively, on catalytically active surface sites or external cocatalysts deployed on the surface. During these processes, there are many possible pathways for recombination of the electron hole pair leading to a wastage of energy, most common being grain boundaries, lattice defects, as well as surface sites, which can be addressed by improving the sample characteristics.[6] However, another important parameter depends on the structural characteristics of the valence and conduction bands. The photogenerated electrons and holes are generally located in conduction and valence bands, respectively, and in most of the semiconductors with bulk 3D structures, they are structurally close to each other enhancing the chances of recombination.[7] Hence, structures with inherent separation of the photogenerated charges spatially, will be ideally placed for efficient photocatalysis. Indeed, such a phenomenon is exploited by nature in utilizing solar energy, whereby the photogenerated charges are separated spatially by cascade processes.[8] Following nature's steps, we can envisage solid oxide structures, which have intrinsic structural anisotropy, leading to separate sites for charge generation and electron conduction pathways, effectively separating holes and electrons.

Lately a lot of attention is garnered by layered semiconductor oxides like $K_4Nb_6O_{17}$,[9] members of Ruddlesden–Popper series of perovskites,[10] layered perovskites, $Sr_2Ta_2O_7$ and $Sr_2Nb_2O_7$, etc. as catalysts for H_2 generation.[11] Typically, these structures consist of sheets of transition metal oxides separated by alkali or alkaline earth metal ions, giving rise to anisotropy to certain extent restricting movement of charges through interlayer spaces. However, in these layered compounds, the attempt is made to introduce catalytic sites within the interlayer spaces, thereby achieving partial space separation of the charges or spatially separate H_2 and O_2 evolution sites reducing the backward reaction. Moreover, high band gap energies of these

Received: April 3, 2014
Accepted: July 1, 2014
Published: July 1, 2014

compounds limit their usage to only UV light region. In this context, we propose the use of structurally anisotropic compounds with photogeneration sites and electron conduction pathways that are spatially separated structurally. To the best of our knowledge, this is the first attempt in efficient visible light driven water splitting by such an anisotropic compound.

We report in this paper structural studies as well as water splitting activity under visible light irradiation of a structurally anisotropic series of compounds, namely, $InFeO_3(ZnO)_m$ (m = 1−4). Isostructural $InGaO_3(ZnO)_m$ compounds are well-known transparent conducting oxides, and structural as well as electronic properties of this series are well-correlated.[12−14] The structure of this series of compounds is fairly complicated, with slabs of InO_6 edge-sharing octahedra separated by blocks of B/ZnO_n polyhedra (where B = Ga, Fe, and Al), which are corner connected to the octahedral slab.[15] Computational studies by Kawazoe and co-workers on the general series $ABO_3(ZnO)_m$, where A is a p-block metal ion, suggest that layers formed by edge-sharing AO_6 octahedra, may act as electron-conducting pathways facilitating electrical conductivity.[16,17] The unique electronic and band structure resulting from such a structural anisotropy makes this series potential materials for addressing recombination issues associated with semiconductor photocatalysts.

EXPERIMENTAL SECTION

Synthesis. A series of compounds of $InFeO_3(ZnO)_m$ (m = 1 to 4) were prepared by means of solid-state synthesis using In_2O_3 (99.99%), Fe_2O_3 (99.99%), and ZnO (99.99%) as starting materials.[18−20] The starting powders with appropriate molar ratios of the oxides corresponding to $InFeO_3(ZnO)_m$ (m = 1 to 4) were thoroughly ground and heated in a platinum crucible progressively to 700, 900, and 1000 °C and kept at each temperature for 12 h. The resulting powders were pressed into pellets and sintered finally at 1350 °C for 12 h with two intermittent grindings.

Characterization. Powder X-ray diffraction (XRD) of all the samples was carried out in a PANalytical X'pert Pro dual goniometer diffractometer working under 40 kV and 30 mA. The radiation used was Cu Kα (1.5418 Å) with a Ni filter, and the data collection was carried out using a flat holder in Bragg−Brentano geometry with 1° slit at the source and receiving sides. An X'celerator solid-state detector with a step size of 0.008° and time per step 43.18 s was employed. Extended X-ray absorption fine structure (EXAFS) measurements on the samples were carried out at the Energy Scanning EXAFS beamline (BL-09) at INDUS-2 synchrotron source at RRCAT, Indore. The specific surface area of the samples was determined by the Brunauer−Emmett−Teller (BET) (adsorption isotherm) method using NOVA 1200 QuantaChrome equipment. The diffuse reflectance UV−visible spectra were recorded on a Cary series UV−vis−NIR spectrometer, in the wavelength range of 200−800 nm.

Catalytic Testing. The catalysts were studied for their photocatalytic activity by reactions that were carried out in a gas-closed system of 70 mL capacity. The photocatalyst powder (50 mg) was dispersed in a reactant solution (25 mL) by a magnetic stirrer in an irradiation cell made of quartz. Typically, 20 mL of pure water and 5 mL of methanol were employed as reactant solutions for water splitting. Here methanol was taken as sacrificial reagent that gets oxidized by the resulting photogenerated holes. Various methanol−water ratios were tried. The light source was 400 W Hg lamp for UV and visible irradiation. The amount of H_2 evolved was determined using gas chromatography (Agilent 7890 GC with Carbosphere column and N_2 as carrier gas) with thermal conductivity detector.

RESULTS AND DISCUSSION

$InFeO_3(ZnO)_m$ (m = 1, 2, 3, and 4 referred to as IFZ1 to 4) are synthesized by solid-state method as modified from the reported procedure. Typically, constituent oxides were ground, pelletized, and heated at a final temperature of 1350 °C in Pt crucibles.

Powder XRD patterns are displayed in Figure 1, which shows highly crystalline diffraction peaks, clearly indicating the

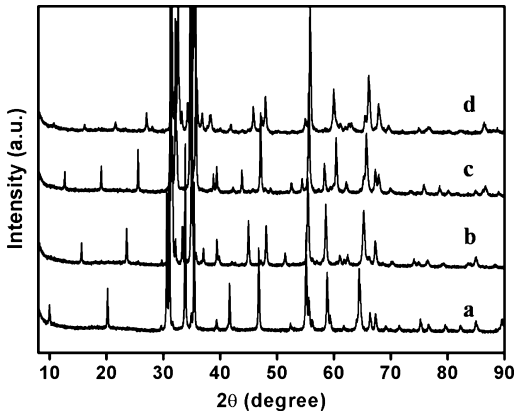

Figure 1. PXRD patterns of $InFeO_3(ZnO)_m$ (a) m = 1, (b) m = 2, (c) m = 3, and (d) m = 4.

formation of required structures (JCPDS Card Nos. 40−0250, 40−0243, 40−024, and 40−0245 for IFZ1, IFZ2, IFZ3, and IFZ4, respectively).[18] Structural or electronic characterization of the Fe analogues of the series, $InBO_3(ZnO)_m$ (B═Ga,Al, and Fe), is rare with most reports focusing on phase studies pointing to similarities in Ga and Al analogues.[18,21] However, we can draw important inferences from isostructural compounds like $InGaO_3(ZnO)_m$, which are structurally well-characterized.[22,13,14] Members of the series in which m is odd are reported to crystallize in rhombohedral phase with space group $R\bar{3}m$, and those with m even crystallize in hexagonal phase with space group $P6_3/mmc$.[23,24] Further structure refinement of the title compounds was carried out based on the crystal data of $InGaO_3(ZnO)_m$ series by Rietveld method using GSAS suite of programs.[25] $ZnFe_2O_4$ phase was added and refined as additional phase as very minor amount of $ZnFe_2O_4$ was detected in XRD studies (Table 1). The atomic positions

Table 1. Impurity Phase Fractions ($ZnFe_2O_4$) in $InFeO_3(ZnO)_m$ (m = 1−4)

compound	impurity phase
IFZ1	3.76%
IFZ2	1%
IFZ3	1.7%
IFZ4	

of pentacoordinated Zn and Fe in IFZ1 and IFZ2 were constrained to be identical with 50% occupancy, and site fractions were constrained to sum to unity. The refinement proceeded more or less smoothly with reasonable refinement parameters. Initially, cell parameters were refined with a few background terms and in a stepwise manner, atomic positions, occupancies, and isothermal parameters were included. After that, profile functions were refined, and again cell parameters, atomic parameters, and isothermal parameters were refined

with increasing background terms. The structural and refinement parameters are tabulated in Table 2, and the patterns with the refinement details and resultant bond lengths are given in the Supporting Information.

Table 2. Refinement and Structural Parameters of $InFeO_3(ZnO)_m$, m = 1−4 (IFZ1, 2, 3, and 4)

parameters[a]	IFZ1	IFZ2	IFZ3	IFZ4
χ^2	4.529	2.368	4.521	7.617
wRp (%)	7.39	5.19	6.44	9.12
Rp (%)	5.39	4.02	4.70	6.32
a (Å)	3.2966(0)	3.3105(0)	3.3057(0)	3.2928(0)
c (Å)	26.0301(6)	22.5871(2)	41.7336(5)	32.9616(0)
Zn1 x	0	0.666 70	0	0.666 70
y	0	0.333 30	0	0.333 30
z	0.216 96	0.365 21	0.739 87	0.091 41
O1 x	0	0.666 70	0	0.666 70
y	0	0.333 30	0	0.333 30
z	0.126 29	0.450 10	0.306 95	0.040 92
O2 x	0	0	0	0
y	0	0	0	0
z	0.290 17	0.345 06	0.085 49	0.1118

[a]In (0,0,0) for all the four compounds; Fe in IFZ1 (0,0, 0.21696), IFZ2 (0,0,0.25), IFZ3 (0,0, 0.13478) and IFZ4 (0.6667,0.33330,0.25); O3 in IFZ2 (0.6667,0.3333,0.25), IFZ3 (0,0, 0.80584) and IFZ4 (0.6667,0.3333,0.17758); O4 in IFZ4 (0,0,0.25); Zn2 in IFZ3 (0,0, 0.13478) and IFZ4 (0,0, 0.17023).

The structure of this family of compounds consists of edge-shared octahedra of indium with oxygen. B and zinc ions occupy trigonal bipyramidal (TBP) or tetrahedral (Td) geometries and form blocks whose thickness is dependent on the number of ZnO layers.

These B/ZnO_n blocks are sandwiched between InO_2 octahedra. The coordination geometry of Zn ions was earlier believed to change between TBP and Td in m odd and even members with Ga site geometry constant in TBP (Figure 2). However, our recent ^{71}Ga magic-angle spinning (MAS) NMR and EXAFS studies in the bulk powder samples, as against single crystals of the earlier studies, evidenced a gradual change of pentacoordination to tetracoordination for both Ga and Zn in the sandwich layer in case of $InGaO_3(ZnO)_m$ as we go across the series with increase in ZnO amount.[26]

These structural characteristics play a pivotal role in rendering these materials as potential candidates for spatial separation of photogenerated charges. Energetically favorable conduction pathways for the electrons are suggested to occur in the InO_6 octahedral layers in $InGaO_3(ZnO)_m$, and charge generation is believed to occur in the sandwich layer comprising of B/ZnO_n coordination geometries.[12,15] Hence structural detail of this region is of paramount importance. The structural studies by PXRD only give an average picture of Zn and Fe coordination, since they may be placed in a random fashion in the sandwich layer. It is desirable to use a technique that can differentiate the local variations in coordination of Zn and Fe separately in the layer.

In view of this, we studied the Zn and Fe coordination characteristics in the sandwich layer in comparison to our earlier studies on $InGaO_3(ZnO)_m$ using EXAFS.[26] At the outset, it is observed that Zn coordination changes from TBP to Td across the series; however, Fe coordination is found to remain in TBP in all the four members. Normalized EXAFS spectra are given in Supporting Information.

Fourier-transformed EXAFS spectra for the $InFeO_3(ZnO)_m$ samples with IFZ1, IFZ2, IFZ3, and IFZ4 measured at Zn edges are shown in Figure 3. The fitted spectra are given in Supporting Information. For m = 1 and m = 2, the EXAFS spectra are fitted with a model where the Zn atom is surrounded by five oxygen atoms. However, for m = 2, Zn is considered in Td structure, whereas for m = 1 the coordination

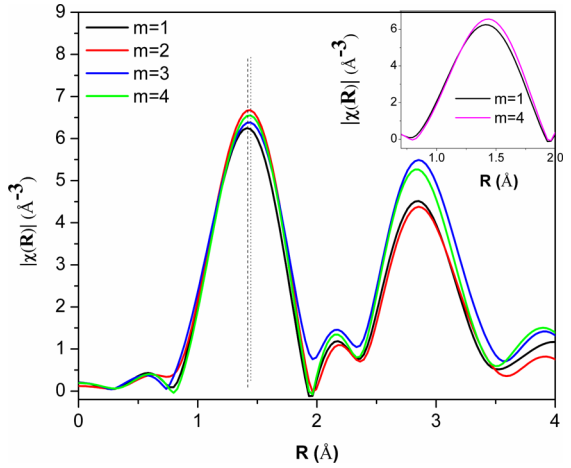

Figure 3. Fourier-transformed EXAFS spectra of $InFeO_3(ZnO)_m$ at Zn K-edge: (black) IFZ1, (red) IFZ2, (blue) IFZ3, and (green) IFZ4. (inset) First coordination shell of m = 1 and 4 compounds.

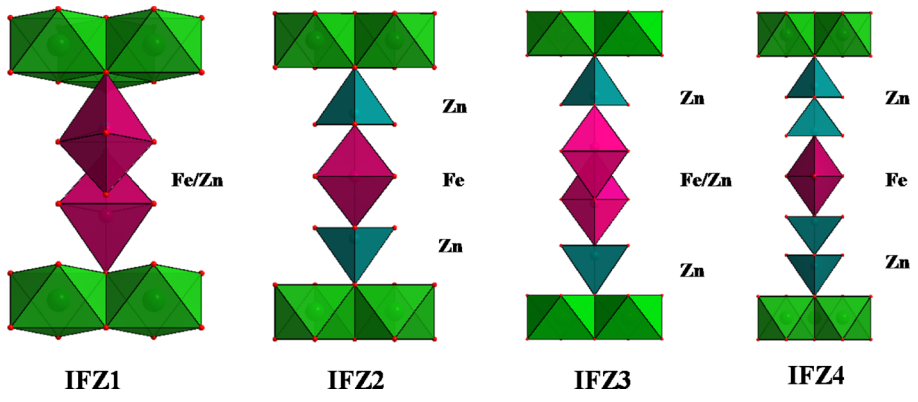

Figure 2. Polyhedral representations of $InFeO_3(ZnO)_m$ (m = 1−4) based on XRD parameters.

is taken as TBP. Zn is found to be pentacoordinated in IFZ1 and IFZ2 with four bonds with lengths ~1.9 Å and a long bond of ~2.3 Å. The contribution of fifth oxygen atom is because of nonbonded oxygen from Fe polyhedra. Better results are obtained when experimental data are fitted with Td Zn sites for both the samples with m = 3 and m = 4 (Supporting Information). Here, Zn occupies Td coordination with bond lengths ranging from 1.82 to 1.94 Å. Note that the contribution of Zn−O coordination in the above spectra (phase not corrected) up to ~2.0 Å is due to the two Zn−O shells. For IFZ3 and IFZ4 this contribution comes from oxygen shells at ~1.9 and 2.0 Å having oxygen coordination of 1 and 3, respectively, for Td structure and 3 and 1 for TBP structure, TBP having another oxygen at 2.3 Å. The first coordination shell, which is shown in the inset of Figure 3 in enlarged scale, is found to shift toward higher R values from m = 1 to m = 4 compounds. Since contributions at higher R values are larger in case of Td structure, samples with higher m value have shown better fitting with Td structure. Note that the FT-EXAFS spectra in the range from 2.0 to 3.5 Å is due to the contributions from further shells of Fe, Zn, and In. Also note that for all the samples, fitting of FT EXAFS spectra was carried out assuming both TBP and Td structures and the best fit results obtained by χ^2 minimization were accepted.

Figure 4 shows the Fourier-transformed EXAFS spectra of all the compounds measured at Fe edges along with the best-fit

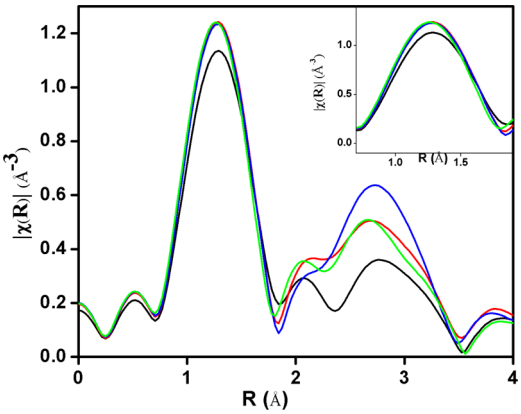

Figure 4. Fourier-transformed EXAFS spectra of $InFeO_3(ZnO)_m$ at Fe K edge: (black) IFZ1, (red) IFZ2, (blue) IFZ3, and (green) IFZ4. (inset) First coordination shell of all the compounds.

theoretical spectra using a model where Fe coordination corresponds to TBP structure. It can be seen from Table 3 that, in all the compounds, Fe is surrounded by three oxygen atoms

Table 3. Local Structural Parameters for $InFeO_3(ZnO)_m$ (m = 1, 2, 3, and 4) Evaluated by EXAFS Measurements at Zn and Fe K-Edge

paths	parameters	IFZ1	IFZ2	IFZ3	IFZ4
Zn−O	R (Å)	1.94	1.96	1.85	1.82
	N	4	4	1	1
Zn−O	R (Å)	2.33	2.36	1.93	1.94
	N	1	1	3	3
Fe−O	R (Å)	1.93	1.91	1.92	1.91
	N	3.09	3.09	3.09	3
Fe−O	R (Å)	2.27	2.23	2.23	2.22
	N	2.2	2	2	2

at a distance of 1.91−1.94 Å and two at a distance of 2.22−2.27 Å. In comparison to the reasonably uniform trigonal bipyramidal bond lengths of Fe, pentacoordinated geometry of Zn seems to be highly distorted with one apical bond shortened subsequently elongating the other apical bond. Note also that the oxygen coordinations in the Fourier-transformed EXAFS spectra mainly contribute up to 1.9 Å. As can be seen from the inset of Figure 4 in enlarged scale, the first peak position is exactly similar in all the four samples, which has led to similar oxygen coordination in all the samples. Only difference is that in case of the m = 1 sample, the first peak amplitude is reduced and its width is increased because of higher σ^2, which indicates structural and thermal disorder. The spectra in the range of 1.9 to 3.5 Å, however, is indeed different from sample to sample, and this is due to contributions from Fe−Fe and Fe−Zn bonds.

Computational studies reported earlier have evidenced that the bottom of the conduction band consists of contributions from In 5s only, and valence band contribution is from O 2p orbitals.[15] It is possible that presence of Fe with partly filled 3d orbitals will lead to a better orbital mixing with the ligand orbitals, and this is observed in case of the pre-edge structure of EXAFS spectrum in Fe K edge. It can be seen from Figure 5

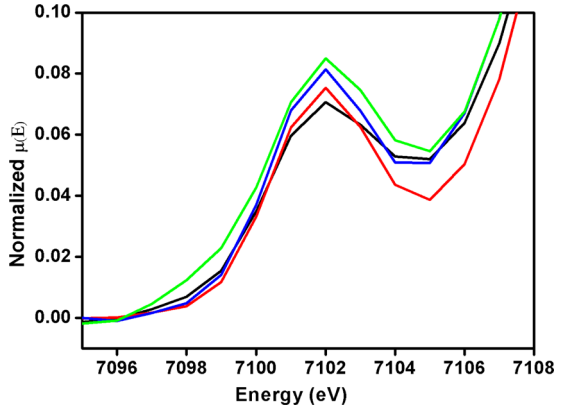

Figure 5. Pre-edge feature in the EXAFS spectra of (black) IFZ1, (red) IFZ2, (blue) IFZ3, and (green) IFZ4.

that the pre-edge feature (1s → 3d/4p transition) is quite prominent and that the peak height is marginally increasing with m. This may be due to slightly enhanced Fe 3d−O 2p mixing although local coordination remains the same. The pre-edge is quite sensitive to the coordination number and orbital geometry and hence may indicate an increase in the coordination of Fe[27] or to a perturbation in the covalent mixing of 3d orbital with ligand valence orbital.[28] The centroids of the pre-edge features for all the samples are at same energy and are coinciding with that of Fe_2O_3 standard sample. This is a clear indication[29] that oxidation state of Fe remains in +3 in all the samples. This would also have an effect in the band gap energies of the compounds. UV−vis absorbance spectra of the series indeed show visible light absorption, which indicates much lower band gap energy compared to their Ga analogues. This may point to some contribution from Fe electronically or structurally.

A relation of reflectance to Kubelka−Munk factor, $F(R) = (1 - R)^2/2R$, was used to calculate the band gap energies. The Kubelka−Munk model forms the basis for measurements of the band gap of bulk powder samples through the construction of

Tauc plot, specifically, a plot of $(F(R)h\nu)^{1/2}$ versus $h\nu$.[30] The band gap energies are estimated in this way to be 2.85, 2.96, 2.97, and 3.022 eV for m = 1−4 compounds, respectively (Figure 6). It is interesting to note that a marginal enhancement of band gap energy occurs with increase in ZnO amount.

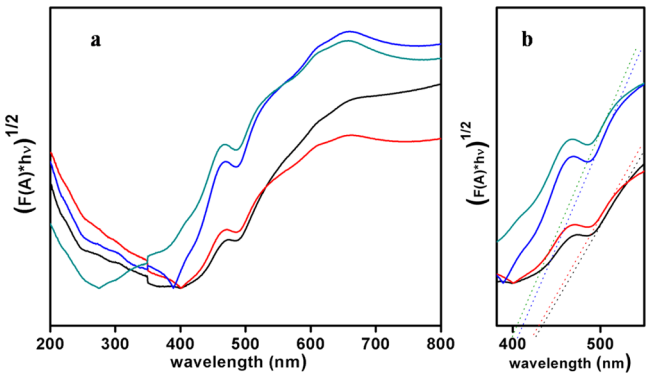

Figure 6. (a) Diffused reflectance spectra of (black) IFZ1, (red) IFZ2, (blue) IFZ3, and (green) IFZ4. (b) The dotted lines indicate band gaps in the visible region.

An attempt in calculating flat band potentials based on Mulliken electronegativity was taken up. This method has been routinely used in calculating band characteristics of simple oxides. Even though structural contributions are not taken into consideration, this method is suggested to give a good understanding even in complex oxides.[31] Details of the calculations are given in Supporting Information, and the band positions are represented in relation with standard hydrogen electrode in Figure 7.

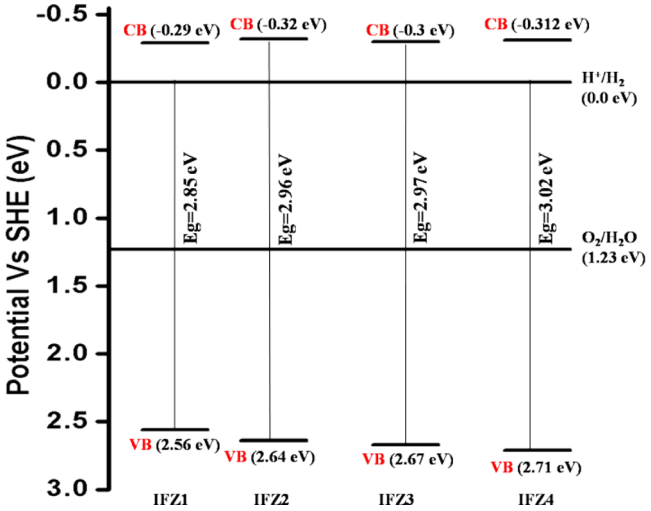

Figure 7. Valence band and conduction band positions of $InFeO_3(ZnO)_m$ (m = 1−4).

It is clear that the conduction band levels of all four compounds are placed energetically close to hydrogen reduction potential, which would be very advantageous in electron transfer and catalysis. Also, it is observed that as ZnO amount increases, valence band values become deeper. An interesting zigzag pattern is observed in the conduction band values with m even members showing slightly enhanced values when compared to m odd members.

The synthesized materials were evaluated for their activity for hydrogen generation from water−methanol mixtures under visible light irradiation. For an optimization of conditions we used 20 mL of water, 5 mL of methanol, and 50 mg of catalyst as a standard under steady-state conditions for irradiation duration of 2 h. On the outset, all four catalysts exhibited very good hydrogen evolution activity (Supporting Information), with standardized hydrogen evolution of ∼19.5 mmol g^{-1} h^{-1} for all the catalysts. The surface areas for IFZ1−4 were estimated from N_2 adsorption studies to be 12.06, 11.54, 11.58, and 11.77 m^2 g^{-1}, respectively. Even though high surface area is usually considered to be ideal for conventional catalysis, in photocatalysis, high crystallinity and consequent reduction in defect sites and surface sites are preferred. Optimization of the methanol volume was also carried out, and an unexpected increase in the hydrogen evolution rate (HER) occurs with 3 mL of methanol (12% v/v methanol in water) as shown in Figure 8. But as the methanol concentration increases further,

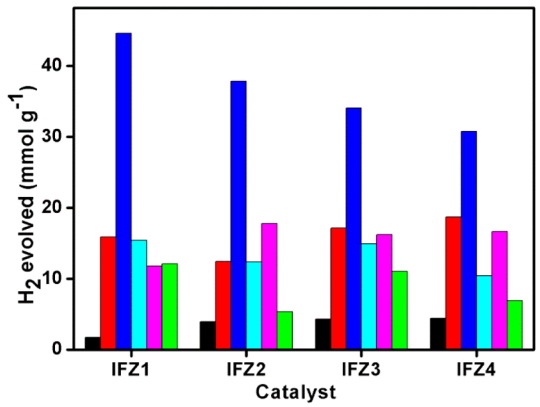

Figure 8. Photocatalytic hydrogen evolution with various methanol−water v/v ratios, (black) 4%, (red) 8%, (blue) 12%, (cyan) 16%, (magenta) 20%, and (green) 24% methanol.

the HER decreases. Stability of the hydrogen evolution was studied under steady-state conditions by following hydrogen evolution rates at different durations (Figure 9).

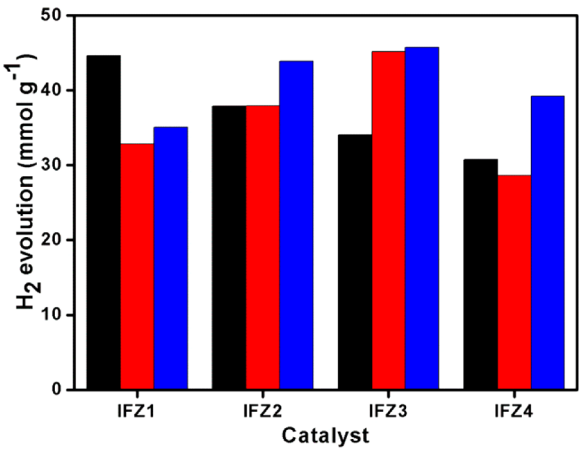

Figure 9. Hydrogen evolution at different reaction time intervals (black) 2 h, (red) 4 h, and (blue) 8 h with 12% v/v methanol−water mixtures.

Interestingly, the hydrogen evolution attains good yields at 2 h and stays stable until 8 h. The saturation in HER is expected due to the steady-state conditions and head space analysis method we followed. Control experiments without methanol, namely, pure water splitting and with IO^{3-}/I^{-} as hole scavenger, did not yield any hydrogen. This shows that methanol not only acts as hole scavenger, but also as electron enricher and contributes to H_2 generation. It is understood that the hole in valence band abstracts a proton from methanol, which forms a radical and injects an electron into the conduction band. This process is called current doubling and can enhance hydrogen production by assisting water splitting.[32] This was also confirmed by observation of CO and CO_2 in our experiments (Supporting Information). The reaction was ascertained to be photocatalytic by absence of H_2 production in dark. Other likely products like formaldehyde and formic acid could not be detected in the reaction mixture. This photocatalytic reaction was also found not to proceed without water ruling out any degradation of methanol as the sole reaction responsible for H_2 generation. The contribution of photocatalytic hydrogen evolution of $ZnFe_2O_4$, the impurity phase fraction present in IFZ1, IFZ2, and IFZ3 was found to be negligible at an evolution rate of only 3.5 mmol g^{-1} h^{-1}.

The crystal structure of the samples remains the same even after the experiments, which is clear from the PXRD (Supporting Information). We could not detect any of the constituent elements in the solution after reaction indicating that the materials are highly stable against photocorrosion or leaching. The higher hydrogen evolution even without the cocatalyst can be attributed directly to the unique structural properties of the compounds. The inherent spatial separation and the low-lying conduction band may be the driving force behind the higher activity. Orbital mixing of Fe 3d orbitals with those of O 2p, may also have contributed to a reduction in band gap energy as well as advantageous band positions. To prove the hypothesis, a mixed oxide system $In_2O_3/Fe_2O_3/ZnO$ was used as the catalyst under same conditions. HER was found to be only 2.7 mmol/g indicating a structural contribution to the enhanced activity of these compounds. Comparison of these results with other layered compounds reported in literature also indicates an unprecedented HER from water−methanol mixtures under visible light irradiation from these anisotropic compounds of the series $InFeO_3(ZnO)_m$. Highest HER in such compounds is reported in UV light for $HCa_2Nb_3O_{10}$ modified with Pt (19 mmol/h/g) from aqueous methanol.[33] NiO loaded $La_2Ti_3O_9$ (Dion−Jacobsen series) is reported to give 0.386 mmol/h/g from aqueous methanol under UV irradiation,[34] whereas a similar compound, $In_2O_3(ZnO)_3$ (m = 3) gives 1.1 μmol/h/g of H_2 from MeOH(aq)/$AgNO_3$ solution under visible light irradiation.[35] H_2 evolution in visible light is scarce, and only 11.2 μmol/h is obtained with 0.3 g of $PbBi_4Ti_4O_{15}$ loaded with Pt in MeOH and $AgNO_3$ as sacrificial reagents.[36]

CONCLUSION

Structurally anisotropic compounds like $InFeO_3(ZnO)_m$ are found to be highly active in H_2 generation from water−methanol mixtures. Structural studies in analogous compounds in the series like $InGaO_3(ZnO)_m$ reveal a layered structure type with InO_6 octahedral layers sandwiching B/ZnO_n polyhedral layers. Computational studies suggest that the InO_6 octahedral layers facilitate fast electron conduction and that charge generation occurs in the sandwich layer. This unique structural feature helps in inherent spatial separation of charge generation sites and electron conduction pathways minimizing charge recombination. Band gap energies observed from UV−vis absorbance spectroscopy indicate visible light absorbance. Flat band potentials are calculated from Mulliken electronegativities, and they show appropriately placed conduction band to enable H_2 evolution. EXAFS studies indicate a possible orbital mixing of Fe 3d and O 2p assisting in Fe contribution to the conduction band and lowering of the band gap conducive for visible light catalytic activity. Methanol in the system acts as hole scavenger as well as facilitates current doubling enhancing H_2 evolution rates. Most of the active catalysts reported are supported noble metal catalysts or use $AgNO_3$ as scavenger. The $InFeO_3(ZnO)_m$ materials are active without employing any cocatalyst, which is also advantageous. Moreover, these compositions are highly conducive for further band gap engineering by isotypical substitution. The catalytic sites also can be varied in this manner, and further insights into the mechanism of H_2 evolution and its dependence on various structural and compositional aspects will pave the way for a novel set of water-splitting catalysts.

ASSOCIATED CONTENT

Supporting Information

Rietveld refinement details, FT-EXAFS fitted spectra, band position calculations from Mulliken electronegativty, activity data, chromatograms, and PXRD pattern of spent catalysts. This material is available free of charge via the Internet at http://pubs.acs.org.

AUTHOR INFORMATION

Corresponding Author

*E-mail: nr.devi@ncl.res.in. Phone: +91 2025902271. Fax: +91 2025902633.

Notes

The authors declare no competing financial interest.

ACKNOWLEDGMENTS

R.N.D. and S.B.N. acknowledge the financial help from NWP56 project under TAPSUN programme funded by CSIR.

REFERENCES

(1) Bard, A. J.; Fox, M. A. Artificial Photosynthesis: Solar Splitting of Water to Hydrogen and Oxygen. *Acc. Chem. Res.* **1995**, *28*, 141−145.
(2) Nowotny, J.; Sorrell, C. C.; Sheppard, L. R.; Bak, T. Solar-Hydrogen: Environmentally Safe Fuel for the Future. *Int. J. Hydrogen Energy* **2005**, *30*, 521−544.
(3) Ni, M.; Leung, M. K. H.; Leung, D. Y. C.; Sumathy, K. A Review and Recent Developments in Photocatalytic Water-Splitting Using TiO_2 for Hydrogen Production. *Renewable Sustainable Energy Rev.* **2007**, *11*, 401−425.
(4) Osterloh, F. E. Inorganic Materials as Catalysts for Photochemical Splitting of Water. *Chem. Mater.* **2008**, *20*, 35−54.
(5) Kudo, A.; Miseki, Y. Heterogeneous Photocatalyst Materials for Water Splitting. *Chem. Soc. Rev.* **2009**, *38*, 253−278.
(6) Istratov, A. A.; Weber, E. R. Electrical Properties and Recombination Activity of Copper, Nickel and Cobalt in Silicon. *Appl. Phys. A: Mater. Sci. Process* **1998**, *66*, 123−136.
(7) Murray, B.; Kagan, C. R.; Bawendi, M. G. Synthesis and Characterization of Monodisperse Nanocrystals and Close-Packed Nanocrystal Assemblies. *Annu. Rev. Mater. Sci.* **2000**, *30*, 545−610.
(8) Nocera, D. G. The Artificial Leaf. *Acc. Chem. Res.* **2012**, *45*, 767−776.

(9) Kudo, A.; Tanaka, A.; Domen, A.; Mayura, K.; Aika, K.; Onishi, T. Photocatalytic Decomposition of Water Over NiO-$K_4Nb_6O_{17}$ Catalyst. *J. Catal.* **1988**, *111*, 67−76.
(10) Jeong, H.; Kim, T.; Kim, D.; Kim, K. Hydrogen Production by the Photocatalytic Overall Water Splitting on NiO/$Sr_3Ti_2O_7$: Effect of Preparation Method. *Int. J. Hydrogen Energy* **2006**, *31*, 1142−1146.
(11) Kudo, A.; Kato, H.; Nakagawa, S. Water Splitting into H_2 and O_2 on New $Sr_2M_2O_7$ (M = Nb and Ta) Photocatalysts with Layered Perovskite Structures: Factors Affecting the Photocatalytic Activity. *J. Phys. Chem. B* **2000**, *104*, 571−575.
(12) Medvedeva, J. E.; Hettiarachchi, C. L. Tuning the Properties of Complex Transparent Conducting Oxides: Role of Crystal Symmetry, Chemical Composition, and Carrier Generation. *Phys. Rev. B* **2010**, *81*, 125116−16.
(13) Keller, I.; Assenmacher, W.; Schnakenburg, G.; Mader, W. Synthesis and Crystal Structures of $InGaO_3(ZnO)_m$ (m = 2 and 3). *Z. Anorg. Allg. Chem.* **2009**, *635*, 2065−2071.
(14) Keller, I.; Mader, W. The Crystal Structure of $InGaO_3(ZnO)_4$: A Single Crystal X-ray and Electron Diffraction Study. *Z. Anorg. Allg. Chem.* **2010**, *636*, 1045−1049.
(15) Orita, M.; Tanji, H.; Mizuno, M.; Adachi, H.; Tanaka, I. Mechanism of Electrical Conductivity of Transparent $InGaZnO_4$. *Phys. Rev. B* **2000**, *61*, 1811−1816.
(16) Omata, T.; Ueda, N.; Ueda, K.; Kawazoe, H. New Ultraviolet-Transport Electroconductive Oxide, $ZnGa_2O_4$ Spinel. *Appl. Phys. Lett.* **1994**, *64*, 1077−1078.
(17) Peng, H.; Song, J. H.; Hopper, E. M.; Zhu, Q.; Mason, T. O.; Freeman, A. J. Possible n−Type Carrier Sources in $In_2O_3(ZnO)_k$. *Chem. Mater.* **2012**, *24*, 106−114.
(18) Kimizuka, N.; Mohri, T.; Matsui, Y. Homologous Compounds,$InFeO_3(ZnO)_m$ (m = 1−9). *J. Solid State Chem.* **1988**, *74*, 98−109.
(19) Zhao, L.; Pei, Y.; Liu, Y.; Berardan, D.; Dragoe, N. $InFeZnO_4$ as Promising Thermal Barrier Coatings. *J. Am. Ceram. Soc.* **2011**, *94*, 1664−1666.
(20) Zhang, C.; Pei, Y.; Zhao, L.; Berardan, D.; Dragoe, N.; Gong, S.; Guo, H. The Phase Stability and Thermophysical Properties of $InFeO_3(ZnO)_m$ (m = 2, 3, 4, 5). *J. Eur. Ceram. Soc.* **2014**, *34*, 63−68.
(21) Kimizuka, N.; Mohri, T.; Nakamura, M. Compounds Which Have $InFeO_3(ZnO)_m$-Type Structures (m = integer). *J. Solid State Chem.* **1989**, *81*, 70−77.
(22) Nespolo, M.; Sato, A.; Osawa, T.; Ohashi, H. Synthesis, Crystal Structure and Charge Distribution of $InGaZnO_4$. X-ray Diffraction Study of 20kb Single Crystal and 50kb Twin by Reticular Merohedry. *Cryst. Res. Technol.* **2000**, *35*, 151−165.
(23) Isobe, M.; Kimizuka, N.; Nakamura, M.; Mohri, T. Structures of $LuFeO_3(ZnO)_m$ (m = 1, 4, 5, and 6). *Acta Crystallogr., Sect. C: Cryst. Struct. Commun.* **1994**, *50*, 332−336.
(24) Li, C.; Bando, Y.; Nakamura, M.; Onoda, M.; Kimizuka, N. Modulated Structures of Homologous Compounds $InMO_3(ZnO)_m$ (M = In, Ga; m = Integer) Described by Four-Dimensional Superspace Group. *J. Solid State Chem.* **1998**, *139*, 347−355.
(25) Toby, B. J. EXPGUI, a Graphical User Interface for GSAS. *Appl. Crystallogr.* **2001**, *34*, 210−213.
(26) Narendranath, S. B.; Yadav, A. K.; Ajithkumar, T. G.; Bhattacharyya, D.; Jha, S. N.; Dey, K. K.; Raja, T.; Devi, R. N. Investigations into Variations in Local Cationic Environment in Layered Oxide Series $InGaO_3(ZnO)_m$ (m = 1−4). *Dalton Trans.* **2014**, *43*, 2120−2126.
(27) Zhao, J.; Huggins, F. E.; Feng, Z.; Huffman, G. P. Ferrihydrite: Surface Structure and Its Effects on Phase Transformation. *Clays Clay Miner.* **1994**, *42*, 737−746.
(28) Westre, T. E.; Kennepohl, P.; Dewitt, J. G.; Hedman, B.; Hodgson, K. O.; Solomon, E. I. A Multiplet Analysis of Fe K-Edge 1s → 3d Pre-Edge Features of Iron Complexes. *J. Am. Chem. Soc.* **1997**, *119*, 6297−6314.
(29) Murphy, A. B. Band-Gap Determination from Diffuse Reflectance Measurements of Semiconductor Films, and Application to Photoelectrochemical Water-Splitting. *Sol. Energy Mater. Sol. Cells* **2007**, *91*, 1326−1337.
(30) Abreu, A. L.; Guimarães, I. R.; Anastáciol, A. S.; Guerreiro, M. C. Natural Goethite Reduced with Dithionite: Evaluation of the Reduction Process by XANES and Mössbauer Spectroscopy and Application of the Catalyst in the Oxidation of Model Organic Compounds. *J. Mol. Catal. A: Chem.* **2012**, *356*, 128−136.
(31) Kim, Y. F.; Atherton, S. J.; Brigham, E. S.; Mallouk, T. E. Sensitized Layered Metal Oxide Semiconductor Particles for Photochemical Hydrogen Evolution from Nonsacrificial Electron Donors. *J. Phys. Chem.* **1993**, *97*, 11802−11810.
(32) Hykaway, N.; Sears, W. M.; Morisaki, H.; Morrison, S. R. Current-Doubling Reactions on Titanium Dioxide Photoanodes. *J. Phys. Chem.* **1986**, *90*, 6663−6667.
(33) Domen, K.; Yoshimura, J.; Sekine, T.; Tanaka, A.; Onishi, T. A Novel Series of Photocatalysts with an Ion-Exchangeable Layered Structure of Niobate. *Catal. Lett.* **1990**, *4*, 339−344.
(34) Kim, J.; Hwang, D. W.; Kim, H. G.; Bae, S. W.; Lee, J. S.; Li, W.; Oh, S. H. Highly Efficient Overall Water Splitting Through Optimization of Preparation and Operation Conditions of Layered Perovskite Photocatalysts. *Top. Catal.* **2005**, *35*, 295−303.
(35) Kudo, A.; Mikami, I. $In_2O_3(ZnO)_m$ Photocatalysts with Laminal Structure for Visible Light-Induced H_2 or O_2 Evolution from Aqueous Solutions Containing Sacrificial Reagents. *Chem. Lett.* **1998**, *10*, 1027−1028.
(36) Kim, H. G.; Becker, O. S.; Jang, J. S.; Ji, S. M.; Borse, P. H.; Lee, J. S. A Generic Method of Visible Light Sensitization for Perovskite-Related Layered Oxides: Substitution Effect of Lead. *J. Solid State Chem.* **2006**, *179*, 1214−1218.